Desalination and Water Treatment
www.deswater.com

doi: 10.5004/dwt.2018.22761

123 (2018) 230–239
August

Ultrasonically induced adsorption of nitrate from aquoeos solution using Fe_3O_4@activated carbon nanocomposite

Afshin Takdastan[a,b], Sudabeh Pourfadakari[b,c,*], Sahand Jorfi[a,b]

[a]*Environmental Technologies Research Center, Ahvaz Jundishapur University of Medical Sciences, Ahvaz, Iran, emails: afshin_ir@yahoo.com (A. Takdastan), sahand369@yahoo.com (S. Jorfi)*
[b]*Department of Environmental Health Engineering, School of Public Health, Ahvaz Jundishapur University of Medical Sciences, Ahvaz, Iran, email: Porfadakar@gmail.com (S. Pourfadakari)*
[c]*Student Research Committee, Ahvaz Jundishapur University of Medical Sciences, Ahvaz, Iran*

Received 27 January 2018; Accepted 14 July 2018

ABSTRACT

The study aimed to evaluate the efficiency of Fe_3O_4@C nanocomposite and ultrasonic (US) waves in removal of nitrate from aqueous solution. In this study, the effect of various parameters influencing nitrate removal, including contact time, pH, nanocomposite dosage, US power, initial nitrate concentration, and temperature, was investigated. The equilibrium adsorption data were analyzed using four common adsorption models. Furthermore, the kinetic and thermodynamic parameters were used to establish the adsorption mechanism. The results of this research revealed a high removal efficiency in pH = 3, equilibrium time = 90 min, and adsorbent dose of 2 g/L. The nitrate removal followed the Langmuir isotherm with R^2 = 0.996 and pseudo-second-order kinetic model (R^2 = 0.996). The thermodynamic parameters indicated that the adsorption of nitrate onto nanocomposite was endothermic and spontaneous. However, this method is important in terms of financial and engineering aspects because of its simple system, low cost, and high removal efficiency.

Keywords: Nitrate; Adsorption; US; Thermodynamic; Fe_3O_4@C nanocomposite

1. Introduction

Increased industrial and agricultural activities have resulted in the generation of toxic pollutants such as inorganic anions. Excessive use of nitrogenous fertilizers in agriculture and discharging untreated industrial wastewater led to contamination of surface and groundwater resources [1,2]. When the concentration of nitrate in drinking water exceeds the limit, it can cause a serious threat to human health manifested through liver damage, cancer, and blue baby syndrome [1,3,4]. Moreover, nitrate discharge in water resources causes eutrophication (algal bloom) phenomenon, which results in the inefficiency of the water resources [5,6]. Hence, the World Health Organization (WHO) set the maximum permissible concentration of nitrate as 50 mg/L in terms of nitrate or 10 mg/L in terms of azote [7]. Also, the Environmental Protection Agency (EPA) has stated the maximum permitted level of nitrate in drinking water 10 mg/L (in terms of nitrate-nitrogen ion) and 50 mg/L in terms of nitrate ion [8]. The Institute of Standards and Industrial Research of Iran has determined nitrate concentration 45 mg/L in terms of nitrate [9]. Therefore, it is essential that nitrate concentration is reduced to a less than the acceptable level. Nitrate ion has a high solubility, so it cannot be easily removed from water [10]. The methods used to remove nitrate include ion exchange, reverse osmosis, chemical reduction, and biological denitrification [11,12]. Most of these methods have disadvantages such as high costs, creating secondary pollution, production of dangerous by-products, difficult exploitation and implementation, pressure drop, problems related to the treatment, and disposal of the produced biological sludge [13,14]. The process of adsorption is taken into consideration because of the low cost, simplicity, and easy governance as

* Corresponding author.

a suitable method for removing contaminants [14]. Many studies have been conducted in the world to use cheaper adsorbents. Activated carbon is one of the known substances, that due to having a large active surface, suitable surface reaction and high porosity to be widely as an adsorbent [15,16]. Unfortunately, the main problem in using powder activated carbon (PAC) or adsorbents with nanosize is isolating them after the adsorption and turbidity in generated wastewater due to the small size of the particles so the distribution and production of secondary pollution is a problem of these systems [17]. Therefore, creating appropriate conditions to facilitate the separation of activated carbon is essential. One of the cheap and fast strategies for this purpose is creating magnetism in activated carbon and their sequestration by magnets. Most recently this method has been widely used because of its simplicity, cost-effectiveness, and high efficiency [18,19]. Fe_3O_4 nanoparticle is widely used due to having several unique properties such as large specific surface area, physical and chemical stability, low toxicity, recyclability, and excellent magnetic features for pollutant removal from water and wastewater [20,21]. In addition, ultrasonic (US) waves are used to enhance the efficiency and speed of reaction and reduce the time. US waves' radiation to the solution surface leads to the formation, development, and collapse of cavitation bubbles. Reactive oxidizing agents such as $O_2^{\bullet-}$, $^{\bullet}H$, $^{\bullet}OH$, and hydrogen peroxide are produced during collapse of the bubbles in high temperature and pressure [22–24]. Ultrasound waves also act as a mixer, causing an increase in the mass transfer between the liquid and solid phase and reducing the particle size and helping to create new active sites on the surface of the Fe_3O_4@C nanocomposite, which improves the distribution of nanocomposite and accelerates the reaction between nitrate and adsorbent [25,26]. So far no studies have been conducted on the removal of nitrate by this nanocomposite in the presence of US waves, therefore the aim of this study was to synthesize and evaluate the efficiency of Fe_3O_4@C nanocomposite and US waves in removing nitrate from aqueous solution.

2. Material and methods

2.1. Materials

The materials used in this study consisted of ferrous sulfate seven water ($FeSO_4.7H_2O$), sodium borohydride ($NaBH_4$) potassium nitrate (KNO_3), polyethylene glycol, ethanol, and sodium hydroxide (NaOH). All chemicals had laboratory purity and were obtained from Merck, Germany. PAC with above 95% purity, specific surface area of (1,027 m^2/g) and pore volume (0.5 cm^3/g), was used as the adsorbent without any further treatment.

2.2. Synthesis of Fe_3O_4 @C nanocomposite

Magnetic nanoparticles were prepared using a liquid phase reduction method according to the technique given by Ranjithkumar et al. [27], with small modifications. At first, powdered activated carbon was washed twice with distilled water and dried overnight at the temperature of 333°K. Then, 1.5 g of $FeSO_4.7H_2O$ and 1.2 g of dried activated carbon were added in 100 mL of distilled water and heated at 323°K for 20 min. Then to this mixture, 100 mL of ethanol 70% and 1 g of polyethylene glycol with constant stirring were added and the reaction pH was adjusted on 7.5 using NaOH (1 M). In the next step, 0.5 g of $NaBH_4$ was added drop by drop to the solution for 3 h to form black colored precipitates. To separate sediments, the suspension was filtered and rinsed with deionized water, and finally, the nitrogen gas furnace with a temperature of 343°K for 24 h was used for drying sediments.

2.3. Characterization Fe_3O_4 @C nanocomposite, PAC

X-ray powder diffraction (XRD) was used in order to determine the magnetic nanocomposition crystalline structures. The XRD patterns were recorded using Rigaku Miniflex diffractometer with Cu Ka radiation at λ = 0.15060 nm, scanning range (2θ): 10°–109°, scanning speed 5°/min, and tube voltage/current 40 kV/30 mA. In addition, surface morphology of the samples was characterized using scanning electron microscopy (Fe-SEM) via a Philips XL 30 electron with an accelerating voltage of 15 kV. Fourier transfer infrared (FTIR) spectra of prepared sample were recorded in vibrational frequency ranging from 4,000 to 400 cm^{-1} using a JASCO 460 plus FTIR spectrometer. Magnetic properties of nanocomposite were determined via a vibrating sample magnetometry (VSM model MDKB).

2.4. Experimental set-up

The experiments were performed in 250 mL glass containers. Sonication was conducted with an ultrasound generator (SONOPULS-HD2200 model, Germany), which was equipped with a 7 mm titanium probe. The tip of the probe was placed 30 mm below the surface of the solution and sonication was performed in an on/off (5 s/5 s) pulse mode at the selected power.

2.5. Experimental procedure

This research was an applicable study that was performed on the synthetic wastewater in a laboratory scale. At the first, nitrate standard solution was made with a concentration of 500 ppm and the rest of concentrations were prepared from dilution of stock solution. HCL and NaOH (0.1 N) were used for adjusting the pH, and the effects of parameters such as contact time (0–120 min), pH solution (3–9), nanocomposite dosage (from 0.4 to 2 g/L), US power (100–400 W), initial nitrate concentration (50–300 mg/L), and temperature (298–313 K) were investigated. After adding the Fe_3O_4@C nanocomposite, samples were US for 10 min. Then, sampling from solutions at specified time intervals was carried out and the nanocomposite was separated from the suspension by magnet under the magnetic field and was immediately washed using a huge amount of deoxygenated water and then dried. Finally, the residual nitrate concentration was analyzed by a spectrophotometer UV-visible (model DR5000) at a wavelength of 220 nm, and the efficiency of the process was determined according to the standard method [28]. Data analysis was performed using Excel software. In this study, using one factor at the varying times, each parameter was separately optimized.

The adsorption capacity of the adsorbent and the removal efficiency were respectively calculated using the following equations [29]:

$$q_t = \frac{(C_0 - C_t)V}{m} \tag{1}$$

$$\mathrm{Re}(\%) = \left(\frac{C_0 - C_t}{C_0}\right) \times 100 \tag{2}$$

where Re is removal efficiency, q_t is the amount of the adsorbed nitrate (mg/g), C_0 is the initial nitrate concentration in the solution (mg/L), C_t is the concentration of the residual nitrate in the solution (mg/L), V is the volume (L), and M is the dose the adsorbent used (g).

2.6. Adsorption studies

In the study, in order to describe nitrate adsorption, isotherm Langmuir, Freundlich, Dubinin–Radushkevich (D–R), and Temkin models were used.

- *Langmuir adsorption isotherm*

Langmuir isotherm is the most applicable adsorption isotherm. Saturated monolayer adsorption is presented through the following equations [30,31]:

$$q_e = \frac{Q_m K_L C_e}{1 + \mathrm{K}_L C_e} \tag{3}$$

The linear form of the Langmuir equation can be written as follows:

$$\frac{1}{q_e} = \frac{1}{Q_m} + \left(\frac{1}{K_L Q_m}\right)\frac{1}{C_e} \tag{4}$$

where q_e is the amount of adsorbed per 1 g of adsorbent and C_e is the amount of remaining material after reaching the state of equilibrium and Q_m is the maximum amount of adsorbed material after reaching the state of equilibrium and K_L is Langmuir constant.

- *Freundlich adsorption isotherm*

The general form of Freundlich equation is shown in the following equation:

$$q_e = K_f C_e^{1/n} \tag{5}$$

where q_e and C_e are similar to items mentioned in Langmuir relation, K and n values are constants which are determined experimentally and are associated with a maximum capacity of bonding and power or traction of bonding, respectively. Freundlich linear form is shown in Eq. (6).

$$\log q_e = \log K_f + \left(\frac{1}{n}\right)\log C_e \tag{6}$$

- *Dubinin–Radushkevich (D–R) adsorption isotherm* is used to determine whether the adsorption process is physical or chemical, and heterogeneity of the surface energies Polanyi potential can be determined via the following equation:

$$\varepsilon = RT\ln\left(1 + \frac{1}{C_e}\right) \tag{7}$$

where ε is the Polanyi potential (J²/mol²), R is the universal gas constant (8.314 J/mol K) and T (K) is the temperature of the solution containing adsorbate molecules.

Isotherm linear form is expressed as follows:

$$\ln q_e = \ln q_s - K_{\mathrm{ad}}\varepsilon^2 \tag{8}$$

where q_s (mol/g) is the maximum sorption capacity, K_{ad} is a constant related to the mean sorption energy (J²/mol²). The constants K_{ad} and q_s can be obtained by plotting of $\ln(q_e)$ versus ε^2. The sorption energy E_s (kJ/mol), which represents the transport free energy of solute the surface of adsorbent calculated by following equation:

$$E_s = \frac{1}{-2\beta^{0.5}} \tag{9}$$

In E_s values between 8 and 16 kJ/mol, the adsorption process would be considered as chemical, while $E_s < 8$ kJ/mol, is a physical adsorption.

- *Temkin adsorption isotherm* contains a factor that considers interactions between adsorbent and adsorbate explicitly (Eq. (10)) is as follows:

$$q_e = \frac{RT}{b}\ln\left(A_T C_e\right) \tag{10}$$

where q_e is the amount of adsorbed per gram of adsorbent.

Temkin isotherm linear form is expressed as follows:

$$q_e = \frac{RT}{b}\ln K_t + \frac{RT}{B}\ln C_e \tag{11}$$

R is the gas constant (8.31 J/mol K), T (K) is the absolute temperature, K_t is equilibrium bond constant (L/mg) associated with the maximum binding energy, and B is constant related to heat of sorption (J/mol). $B = RT/b$ and K_t are constants in this study. Isotherm constants (B, K_t) are obtained from the slope and intercepting of q_e graph against $\ln C_e$.

2.7. Kinetic studies

Kinetic studies are used for designing and modeling the processes and the reactions performed in the reactor. In this research, pseudo-first-order and pseudo-second-order models were utilized [32,33].

- *Pseudo-first-order Eq. (12):*

$$\frac{dq_t}{dt} = k_1\left(q_e - q_t\right) \tag{12}$$

The linear pseudo-first-order equation is given as:

$$\log\left(q_e - q_t\right) = \log\left(q_e\right) - \frac{k_1}{2.303}t \tag{13}$$

where q_e and q_t (mg/g) are the amounts of nitrate adsorbed on the adsorbent at equilibrium time and at the time of t, respectively, k_1 is the equilibrium rate constant of pseudo-first-order (min^{-1}), and t is the contact time (min). The slope and intercept of the plot of log $(q_e - q_t)$ versus t were used to determine the pseudo-first-order rate constant.

- *Pseudo-second-order Eqs. (14 and 15):*

$$\frac{dq_t}{dt} = k_2\left(q_e - q_t\right)^2 \tag{14}$$

The linear pseudo-second-order equation is given as:

$$\frac{t}{q_t} = \left(\frac{1}{k_2 q_e^2}\right) + \left(\frac{1}{q_e}\right)t \tag{15}$$

where K_2 (g/mg min) is the rate constant of pseudo-second-order model for adsorption. The values K_2 and q_e were calculated from the plot of t/q_t versus t.

3. Results and discussion

3.1. Characterization of Fe_3O_4 @C nanocomposite

The Fe-SEM images and EDX of the nanocomposite and PAC taken at different magnifications are shown in Figs. 1(a) and (b). Nanocomposite images in Fig. 1(a) show that nanoparticles are spherical with well-dispersed and average particle size is (13.12–19.41 nm). The chemical composition of the magnetic nanoparticles was analyzed by EDX. The quantitative analysis indicated the molar presence of carbon (59.33%), oxygen (35.69%), and iron (14.98%) in the nanocomposite. Also, Fig. 1(b) shows a uniform distribution of PAC with particle size ranging from 18.69 to 19.47 nm, the elemental analysis shows the molar presence of carbon (86%) and oxygen (13%) in PAC. These materials consist mainly of pure carbon walls with a small amount of oxygen-containing functional groups. Powder X-ray diffraction patterns of the synthesized MNPs and PAC are shown in Figs. 2(a) and (b). The XRD spectra in Fig. 2(a) revealed small peaks at 2θ = 53.52° and 62.43°, while main dominant peaks of nanocomposite were observed at 2θ of 26.17° and 35.68° which is related to the existence of adsorbent crystalline phases and it is in good agreement with the standard JCPDS card no (98-007-7842). Also, according to XRD analysis in Fig. 2(b), the results revealed that small peaks are located at 2θ = 29.66° with d spacing 2.04051Å, and main dominant peaks of PAC were observed at 2θ of 23.52 and 26.53°, which is in good agreement with the standard JCPDS card no (00-050-0926). The FTIR spectra of Fe_3O_4@C nanocomposite are shown in Fig. 3(a), it can be seen that adsorption band at 470.34 cm^{-1} related to Fe-O functional group on the surface of nanocomposite, the stretching vibration of C = O is observed in 1,633.06 and 1,726 cm^{-1}. The adsorption peaks observed at 3,433.6 and 3,759.8 cm^{-1} could be assigned to the OH. The peaks at 2,856 and 2,923 cm^{-1} related to CH stretching, the intense bands at 1,086–1,328 cm^{-1} can be attributed to stretching of C–O [34]. Therefore, it can be concluded that the Fe3O4@Cnanocomposite was effectively coated by the PAC. Magnetic characterization of the nanocomposite was determined using (VSM) at room temperature. According to Fig. 3(b), it shows that magnetic saturation value is 0.9 emu/g for Fe_3O_4@C nanocomposite, it can be concluded that the decrease of saturation magnetization is due to the existence of PAC on the surface of Fe_3O_4 [35].

3.2. Effect of operational parameters

3.2.1. The effect of pH value

Fig. 4(a) shows the effect of pH on the uptake of nitrate with initial concentration of 100 mg/L, nanocomposite dose (0.4 g/L) in contact time (0–120 min), and US power of 100 W. According to this figure, by increasing the contact time, the nitrate removal efficiency increased during initial 60 min and after this time the adsorption amount increased with a mild slope until reaching the equilibrium (about 90 min). Also, the results obtained showed that with increasing pH from 3 to 9, in contact time 90 min, nitrate removal efficiency reduced from 57.1% to 33.1%, respectively, and the maximum removal was obtained in pH = 3. The reason of increased efficiency removal of nitrate in low pH is the increasing of ion H^+ in the environment and decreasing of ion OH^-. Because in low pH, the electrostatic attractions increase between nitrate

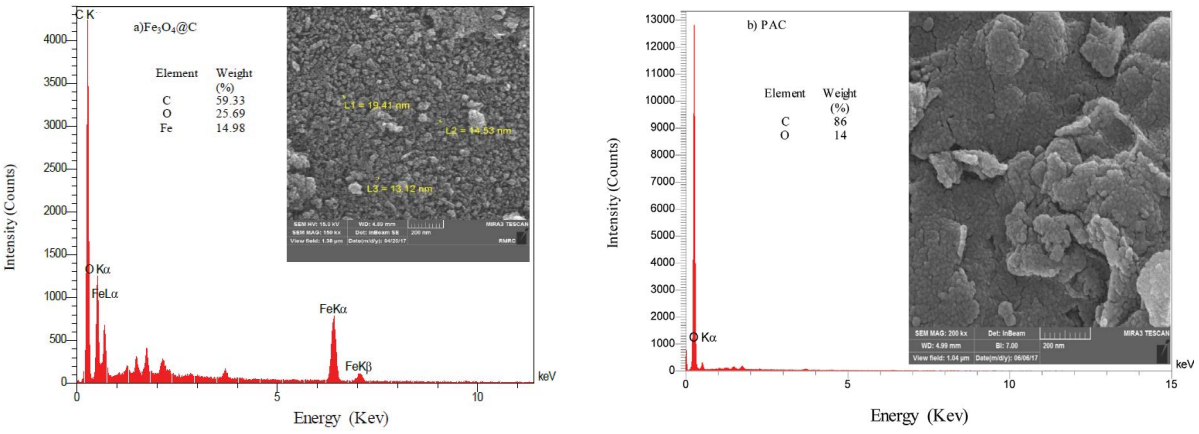

Fig. 1. Fe- SEM images and EDX of (a) Fe_3O_4@C and (b) (PAC).

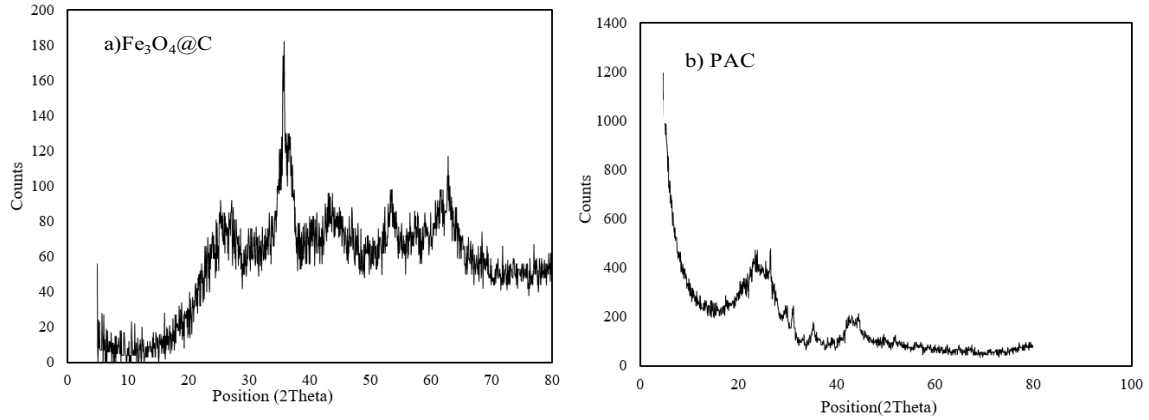

Fig. 2. XRD patterns of (a) Fe_3O_4@C and (b) PAC.

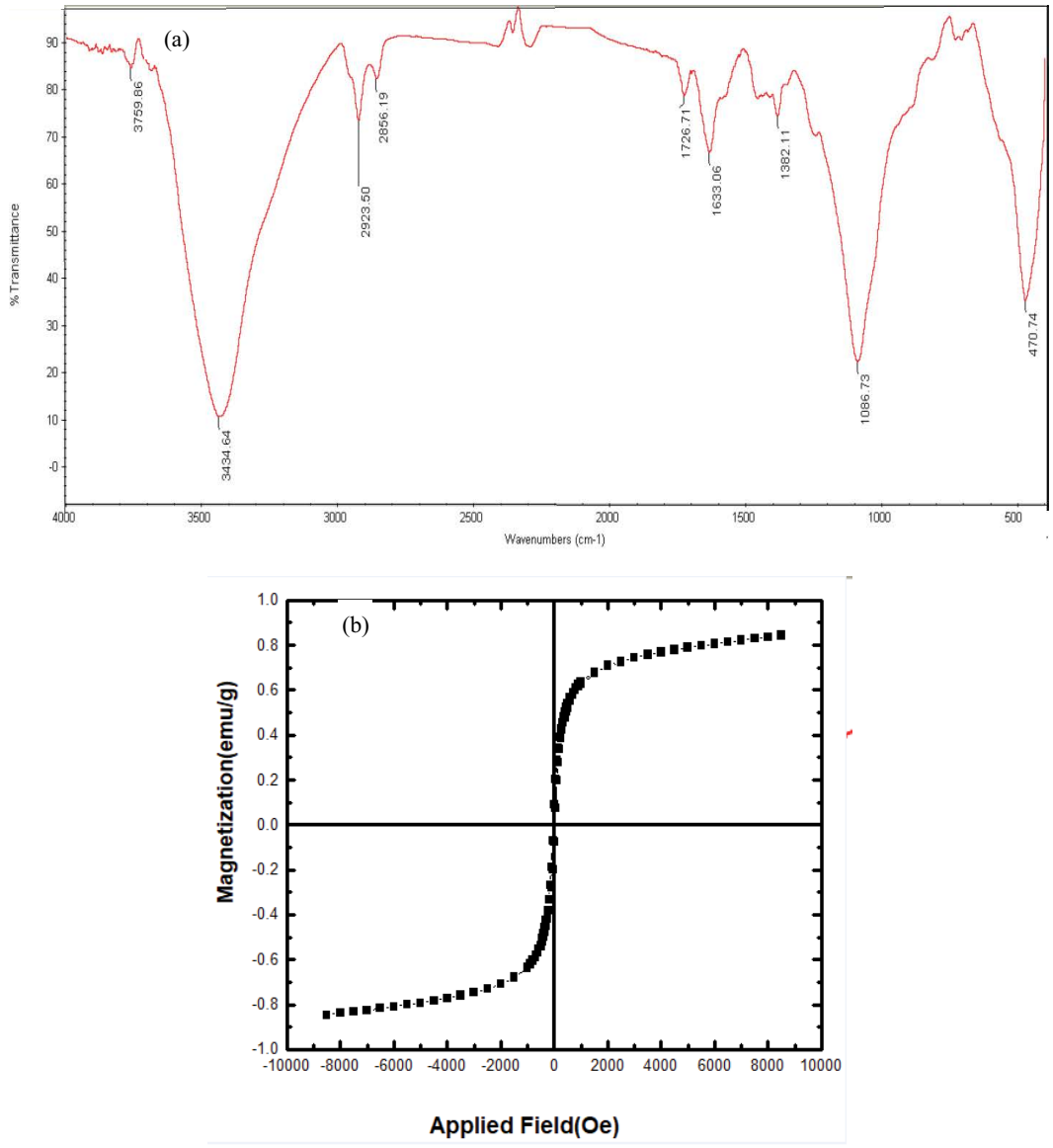

Fig. 3. (a) FTIR pattern and (b) VSM of Fe_3O_4@C nanocomposite.

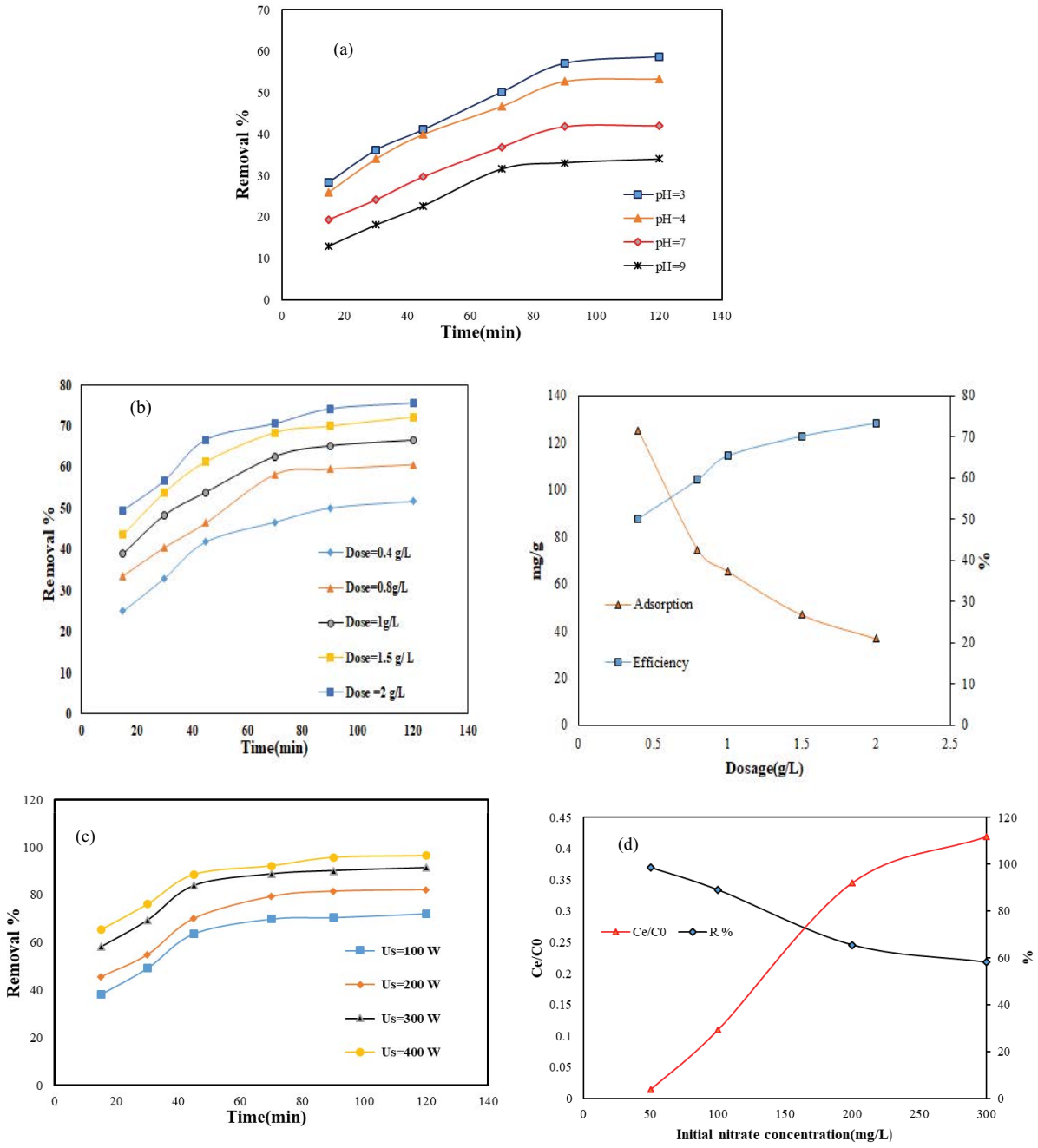

Fig. 4. Effects of different parameters on nitrate removal using Fe_3O_4@C/US process, (a) effect of initial solution pH (nanocomposite dose: 0.4 g/L, US: 100 W, nitrate concentration of 100 mg/L), (b) effects of Fe_3O_4@C nanocomposite dosage (pH = 4, US: 100 W, nitrate concentration of 100 mg/L), (c) effects of US power (frequency: 35 kHz, pH = 4, nitrate concentration: 100 mg/L, nanocomposite dosage: 1.5 g/L), and (d) effects of initial nitrate concentration (pH 4, nanocomposite dose: 1.5 g/L, US: 300 W).

molecules (negative charge) and the adsorbent surface (positive charge) and the amount of adsorption of contaminant increases on the adsorbent surfaces. In other words, the charge on the surface of the adsorbent is affected by the pH of the solution [36,37]. This finding is similar to literature Zhu et al. [38]. In this study, due to the little difference in the amount of nitrate removal between pH 4 and 3 in terms of efficiency, pH = 4 has been considered as the optimal pH. The pH_{pzc} was taken as the point which the net electric charge on the adsorbent surface is zero. For Fe_3O_4@C nanocomposite, the pH_{pzc} (point of zero charge) is 5.5, suggesting that the surface charge of Fe_3O_4@C nanocomposite is negative at pH > pH_{pzc}, and positive at pH < pH_{pzc}. Moreover, the adsorption speed was fast during the first 60 min and then, it followed a steady slope and reached equilibrium after 90 min. The reason is that at the primary stages of adsorption, a large number

of blank area on the surface of Fe_3O_4@C nanocomposite is available that with the passage of time is occupied by nitrate molecules and the removal efficiency after the balance time remains constant [39].

3.2.2. The effect of Fe_3O_4@C nanocomposite dosage

In order to determine the effect of the dosage of nanocomposite on the nitrate removal, different amounts of nanocomposite (0.4–2 g/L) were added to 100 mg/L of initial nitrate concentration at pH = 4 and US power of 100 W. According to Fig. 4(b), the obtained results showed that by increasing the dose of nanocomposite from 0.4 to 1.5 g/L, the removal efficiency increased from 50.1% to 70.1%, and in dose 2 g/L, removal efficiency reached to 74.3%. Also, the adsorption capacity decreased from 125.25 to 46.73 mg/g and in dose 2 g/L reached 36.65 mg/g. However, the addition of more amount of adsorbent had little impact on increasing the amount removed of nitrate, thus the dose of 1.5 g/L as the nanocomposite optimal dose was considered. Increase in the removal rate by increasing the dose is due to increasing adsorption unsaturated active sites on adsorbent surface which are occupied by nitrate anions [1]. Bhaumik et al. [40] studied Cr (VI) removal with polypyrrole/Fe_3O_4, and the results showed that by increasing adsorbent dose from 0.025 to 1 g/L the removal percentage increased.

3.2.3. The effect of ultrasonic power

To evaluate the effect of US power on nitrate removal, experiments were conducted using Fe_3O_4@C nanocomposite dose of 1.5 g/L at pH = 4 and different US power (100–400 W) in a fixed frequency 35 kHz. According to Fig. 4(c), it is clear that nitrate removal efficiency increased with increasing US power and these changes are most evident when the US power rises from 100 to 400, so that after 90 min, the removal efficiency increased from 70.5% to 95.1% for concentration 100 mg/L of nitrate. The reason is that with increasing US power intensity of mixing between the adsorbent and solution increases due to the production of turbulence by the collapse of cavitation bubbles [24,25]. In this study, to save energy consumption, US power 300 W was determined to continue testing. Results of current study in terms of US power effects are in accordance with literature [41].

3.2.4. The effect of initial nitrate concentration

The effect of initial nitrate concentration was evaluated using nanocomposite dose of 1.5 g/L at pH 4 and US with a power of 300 W at different concentrations of nitrate (50–300 mg/L). The results obtained in Fig. 4(d) show that by decreasing the initial nitrate concentration of 300–50 mg/L, removal efficiency increased from 58.1% to 98.6%. In addition, the adsorption ion capacity decreased from 116.2 to 32.86 mg/g. Because in the fixed amount of adsorbent, most of the nitrate molecules are adsorbed on the surface of adsorbent and most of the adsorption sites are saturated. Also, increased in adsorption capacity is due to an increase in the driving force of the concentration gradient with the increase in the initial concentration [42]. In another recent study by Moradi et al. [43] on removal of Pb (ii) ions using magnetic nanocomposite, the results obtained shown that by increasing concentration, the removal efficiency decreased from 99% to 44%.

3.2.5. Comparison of Fe_3o_4@C/US, PAC and US processes for nitrate removal

In Fig. 5, the effect three processes (Fe_3O_4@C, US, and PAC) on removal nitrate have been shown. It is obvious that the removal efficiency of nitrate through Fe_3O_4@C/US process was higher than other processes. Therefore, according to results it is clear that the use of US waves can reduce contact time and increase removal efficiency. Also, several researchers have investigated about the removal efficiency of nitrate shown in Table 1.

3.3. Adsorption isotherms and kinetics

To determine isotherm models and to evaluate the capacity of nitrate adsorption, the adsorption experiments were performed in glass containers 200 mL, with the addition of Fe_3O_4@C nanocomposite optimized dose. The solutions of each container were placed in Shaker incubator with 150 rpm and the temperature of 303°K and the samples were taken after 2 h and the amount of adsorption capacity was determined. The results of the four isotherms and their correlation coefficients are shown in Table 2. According to the results obtained from isotherm studies, it is obvious that Langmuir isotherm model with $R^2 = 0.996$ had a better correlation compared with the other isotherms and the capacity of equilibrium adsorption was gradually increased by increasing the equilibrium concentration of nitrate, and maximum adsorption capacity of magnetic nanocomposite was obtained as 116.2 mg/g. The reason for this is easy access to adsorption sites in the early stages of the process. The values of n in the range of 1–10 show which adsorption was favorable. The result obtained of the Freundlich isotherm indicates the constant n was greater than 1, which represents the favorable removal conditions. Furthermore, the value of E obtained of D–R isotherm was calculated 16.6 kJ/mol, which showed

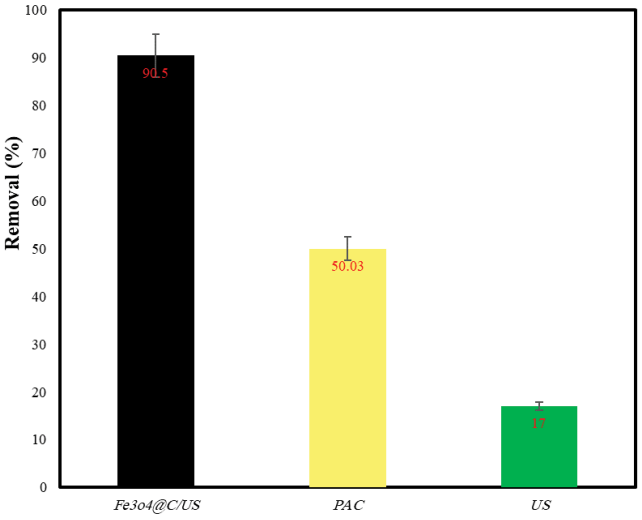

Fig. 5. Comparison of Fe_3o_4@C, PAC and US processes for nitrate removal in optimum condition.

Table 1
Comparison the results of this study and done studies

Compound	Process	Removal (%)	References
Nitrate	Ze-NZVI at (pH = 5.5)	84	[44]
Nitrate	Clinoptilolite	8.7	[45]
	Activated carbon	62.6	[45]
Nitrate	Almond shells activated with magnetic nanoparticles at (pH = 5.5)	76.29	[46]
Nitrate and phosphate	Clinoptilolite-supported iron hydroxide at (pH = 2)	81–93	[47]
Nitrate	Fe_3O_4@C/US at (pH = 4)	90.1	This study

Table 2
The results of the study of adsorption isotherms

Type of isotherm model	Parameters	Value
Langmuir	Q_m (mg/g)	90.9
	K_a (L/mg)	0.3
	R^2	0.996
Freundlich	K_F (mg/g)	34.67
	n	4.34
	R^2	0.986
Dubinin–Radushkevich (D–R)	q_m (mol/g)	170
	E (kJ/mol)	16.6
	R^2	0.97
Temkin	b_t	622
	K_T (L/mg)	7.59
	R^2	0.88

the adsorption of nitrate onto nanocomposite was chemical mechanism. To determine the kinetic models, adsorption kinetics experiments were performed in 200 mL glass containers containing adsorbent dose of 1.5 g/L and initial nitrate concentration 100 mg/L to determine the minimum time required to achieve anion adsorption in constant and uniform conditions at pH = 4. The obtained results from examining kinetic models in Table 3 show that pseudo-second-order kinetic equation is the best model to determine the reaction rate (R^2 = 0.996). Adsorption equilibrium curve and pseudo-second-order kinetic equation curve are shown in Figs. 6(a) and (b). The results of the study conducted by Öztürk et al. [48] on removing nitrate by powdered activated carbon, showed that nitrate adsorption followed a pseudo-second-order kinetics model with R^2 = 0.999.

3.4. The effect of temperature

Fig. 7 shows the effect of temperature on the nitrate adsorption process in different temperatures using adsorbent

Table 3
The results of studying the kinetics

Type of kinetic model	Parameter	Value
Pseudo-first-order	k_1 (min^{-1})	0.047
	$q_e$cal (mg/g)	58.85
	R^2	0.962
Pseudo-second-order	k_2 (min^{-1})	0.001
	$q_e$cal (mg/g)	67.4
	h	4.99
	R^2	0.996

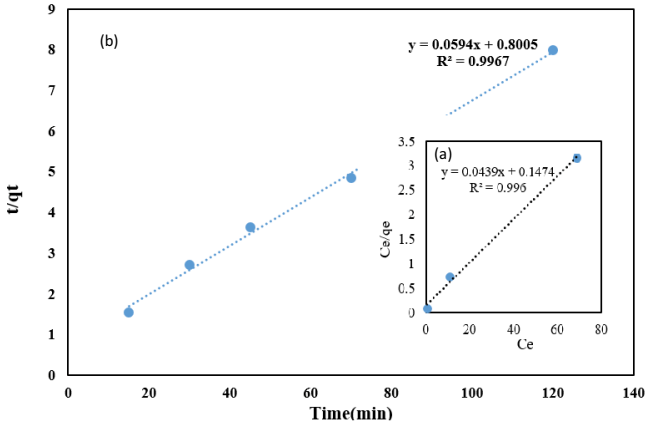

Fig. 6. Modeling (a) Langmuir adsorption isotherm and (b) pseudo-second-order kinetic model for nitrate adsorption.

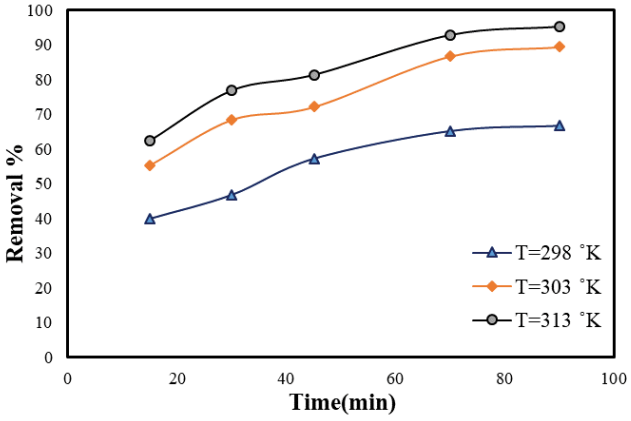

Fig. 7. Effect of the temperature on nitrate removal (ultrasonic power: 300 W pH: 4, adsorbent dosage: 1.5 g/L) at different times.

dose of 1.5 g/L, pH = 4, and initial nitrate concentrations 100 mg/L. The results obtained showed that by increasing the temperature from 298 to 313 K, removal efficiency increased from 66.6% to 95.2%. Also, in order to determine thermodynamic parameters, experiments were carried out at three different temperatures for nitrate removal. The thermodynamic parameters standard free energy (ΔG°), enthalpy change (ΔH°), and entropy change (ΔS°) were estimated

to evaluate the exothermic or endothermic nature of the adsorption process. The Gibb's free energy change (ΔG^0) can be calculated by the following equations [49,50]:

$$\Delta G^\circ = -RT\ln\left(K_L\right) \tag{16}$$

$$\Delta G^\circ = \Delta H^\circ - T\Delta S^\circ \tag{17}$$

$$\ln\left(K_L\right) = \left(\frac{\Delta S^\circ}{R}\right) - \left(\frac{\Delta H^\circ}{RT}\right) \tag{18}$$

where K_L is equilibrium constant (mol^{-1}), R is the gas constant (8.314 J/mol K), T is the temperature (K). The values of enthalpy change (ΔH°) and entropy change (ΔS°) were calculated from the slope and intercept of the plot of ln K_L versus ($1/T$). The results of these thermodynamic parameters are given in Table 4. According to results, the negative values of ΔG° indicate the spontaneous nature of adsorption at higher temperatures. Positive value of ΔH° indicates that the adsorption process is endothermic nature and positive value of ΔS° shows the increase in the degree of freedom at the solid–liquid interface during nitrate adsorption [51].

3.5. Desorption study

For the reusability of Fe_3O_4@C nanocomposite, adsorption/desorption cycles were done using a methanol solution (60%, V/V). Hence, nanocomposite was immersed in methanol for 30 min, then washed by Milli-Q water and was dried in furnace for further use. The results obtained from Fig. 8 show that the removal of nitrate by nanocomposite, decreased slightly after four cycles and from 73.5% reached 34.6%, hence application of Fe_3O_4@C nanocomposite, in removal of nitrate and other pollutant is suggested.

Table 4
Thermodynamic parameters at different temperatures

T (K)	ΔG° (kJ/mol)	ΔS° (kJ/mol)	ΔH° (kJ/mol)
298	–24.3	0.38	111.9
303	–24.8		
313	–25.5		

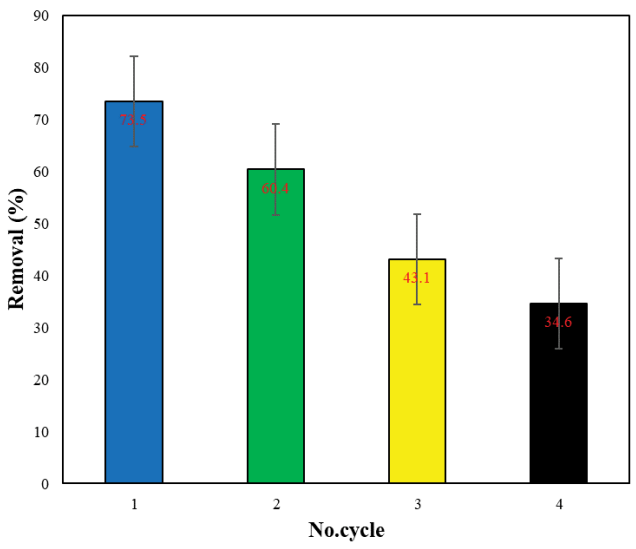

Fig. 8. Desorption of Fe_3O_4@C using methanol solution for nitrate ion removal (initial concentration 100 mg/L).

4. Conclusions

In the current study, the magnetic nanocomposite of Fe_3O_4@C was successfully synthesized and used in the removal of nitrate from aqueous environments. Modified activated carbon with the Fe_3O_4 nanoparticle is more efficient in nitrate removal because of the adsorption sites increased on adsorbent surface. The adsorption results showed that increasing contact time and initial nitrate concentration led to enhancing the adsorption as mg/g. Also, Freundlich isotherm and pseudo-second-order kinetic model are the best models for describing the nitrate adsorption reaction on magnetic nanocomposite of Fe_3O_4@C. However, this method is important from the perspective of economic and engineering because of the simple system, low cost, and removal high efficiency.

Acknowledgment

This research project has been financially supported by the Environmental Technologies Research Center, Ahvaz Jundishapur University of Medical Sciences (grant no ETRC 9611).

References

[1] M. El Ouardi, S. Qourzal, S. Alahiane, A. Assabbane, J. Douch, Effective removal of nitrates ions from aqueous solution using new clay as potential low-cost adsorbent, J. Encap. Adsorp. Sci., 5 (2015) 178–190.
[2] P. Loganathan, S. Vignswaran, J. Kandasamy, Enhanced removal of nitrate from water using surface modification of adsorbents—a review, J. Environ. Manage., 131 (2013) 363–374.
[3] J. Luo, S. Guangren, J. Liu, G. Qian, Z. Ping Xu, Mechanism of enhanced nitrate reduction via micro-electrolysis at the powdered zero-valent iron/activated carbon interface, J. Colloid Interface Sci., 435 (2014) 21–25.
[4] M. Chabani, A. Amrane, A. Bensmaili, Equilibrium sorption isotherms for nitrate on resin amberlite IRA 400, J. Hazard. Mater., 165 (2009) 27–33.
[5] D. Majumdar, Nitrate pollution of groundwater and associated human health disorders, Ind. J. Environ. Health, 42 (2000) 28–39.
[6] G.R. Shaw, D.P. Moore, C. Garnett, Eutrophication and algal blooms, Environ. Ecol. Chem., 2 (2003) 1–21.
[7] WHO, Guidelines for Drinking Water Quality, 3rd ed., WHO, Geneva, 2008.
[8] U.E.P.A., USEPA National Primary and Secondary Drinking Water Regulations, USEPA, USA, 2008.
[9] ISIRI, Institute of Standards and Industrial Research of Iran, Drinking Water—Physical and Chemical Specifications, 5th ed., Tehran, 1053, 2009.
[10] M. Islam, P.C. Mishra, R. Patel, Physicochemical characterization of hydroxyapatite and its application towards removal of nitrate from water, J. Environ. Manage., 91 (2010) 1883–1891.
[11] S. Chatterjee, D.S. Lee, M.W. Lee, S.H. Woo, Nitrate removal from aqueous solutions by cross-linked chitosan beads conditioned with sodium bisulfate, J. Hazard. Mater., 166 (2009) 508–513.

[12] N. Öztürk, T.E. Bektas, Nitrate removal from aqueous solution by adsorption onto various materials, J. Hazard. Mater., 112 (2004) 155–162.
[13] S. Pourfadakari, N. Yusefi, A.H. Mahvi, Removal of Reactive Red 198 from aqueous solution by combined method multi-walled carbon nanotubes and zero-valent iron: equilibrium, kinetics, and thermodynamic, Chin. J. Chem. Eng., 24 (2016) 1448–1455.
[14] M.A. Baghapour, S. Pourfadakari, A.H. Mahvi, Investigation of Reactive Red Dye 198 removal using multiwall carbon nanotubes in aqueous solution, J. Ind. Eng. Chem., 20 (2014) 2921–2926.
[15] M.A. Baghapour, A.H. Mahvi, S. Pourfadakari, Thermodynamic analysis of reactive red 198 removal from synthetic wastewater by using multiwall carbon nanotubes, Health Scope, 2 (2013) 149–155.
[16] A. Takdastan, A.H. Mahvi, E.C. Lima, A.A. Babaei, G. Goudarzi, A. Neisi, M. Heidari Farsani, M. Vosoughi, Preparation, characterization, and application of activated carbon from low-cost material for the adsorption of tetracycline antibiotic from aqueous solutions, Water Sci. Technol., 74 (2016) 2349–2363.
[17] B. Kakavandi, J. Jafari, R.K. Rezaei, S. Nasseri, A. Ameri, A. Esrafily, Synthesis and properties of Fe_3O_4-activated carbon magnetic nanoparticles for removal of aniline from aqueous solution equilibrium, kinetic and thermodynamic studies, Iranian J. Environ. Health Sci. Eng., 10 (2013) 2–9.
[18] S. Pourfadakari, A.H. Mahvi, Kinetics and equilibrium studies for removal of reactive red 198 from aqueous solutions using zero valent iron powder, Health Scope, 3 (2014) 1–8.
[19] X. Zhao, J. Wang, F. Wu, Th. Wang, Removal of fluoride from aqueous media by Fe_3O_4@$Al(OH)_3$ magnetic nanoparticles, J. Hazard. Mater., 173 (2010) 102–109.
[20] M.H. Do, N.H. Phan, Th.D. Nguyen, Activated carbon/Fe_3O_4 nanoparticle composite: fabrication, methyl orange removal and regeneration by hydrogen peroxide, Chemosphere, 85 (2011) 1269–1279.
[21] Z. Liu, F.Sh. Zhang, R. Sasai, Arsenate removal from water using Fe3O4 loaded activated carbon prepared from waste biomass, J. Chem. Eng., 160 (2010) 57–62.
[22] Ch. Cai, H. Zhang, X. Zhong, L. Ho, Ultrasound enhanced heterogeneous activation of peroxymonosulfate by a bimetallic Fe–Co/SBA-15 catalyst for the degradation of Orange II in water, J. Hazard. Mater., 283 (2015) 70–79.
[23] H. Yanagida, Y. Masubuchi, K. Minagawa, T. Ogata, J.-I. Takimoto, K. Koyama, A reaction kinetics model of water sonolysis in the presence of a spin-trap, Ultra Sonochem., 5 (1999) 133–139.
[24] H. Ghodbane, O. Hamdaoui, Degradation of Acid Blue 25 in aqueous media using 1700kHz ultrasonic irradiation: ultrasound/Fe (II) and ultrasound/H_2O_2 combinations, Ultra Sonochem., 16 (2009) 593–598.
[25] S. Ghodke, S. Sonawane, R. Gaikawad, K.C. Mohite, TIO_2/Nanoclay nanocomposite for phenol degradation in sono-photocatalytic reactor, J. Chem. Eng., 90 (2012) 1153–1159.
[26] Y.L. Pang, A.Z. Abdullah, S. Bhatia, Review on sonochemical methods in the presence of catalysts and chemical additives for treatment of organic pollutants in wastewater, Desal. Wat. Treat., 277 (2011) 1–14.
[27] V.H. Ranjithkumar, A.N. Hazeen, M. Thamilselvan, S. Vairam, Magnetic activated carbon-Fe_3O_4 nanocomposites—synthesis and applications in the removal of acid yellow dye 17 from water, J. Nanosci. Nanotechnol., 14 (2014) 4949–4959.
[28] A. APHA, WEF, Standard Methods for Examination of Water and Wastewater, APHA, Washington, DC, 2005.
[29] N. Jaafarzadeh, A. Takdastan, M. Heidari Farsani, N. Niknam, M. Aalipour, M. Hadei, P. Bahrami, Biosorption of heavy metals from aqueous solutions onto chitin, Int. J. Environ. Health Eng., 4 (2015) 1–6.
[30] A.O. Dada, A.P. Olalekan, A.M. Olatunya, Langmuir, Freundlich, Temkin and Dubinin–Radushkevich isotherms studies of equilibrium sorption of Zn^{2+} unto phosphoric acid modified rice husk, IOSR-JAC, 3 (2012) 38–45.
[31] S. Pourfadakari, S. Jorfi, M. Ahmadi, A. Takdastan, Experimental data on adsorption of Cr(VI) from aqueous solution using nanosized cellulose fibers obtained from rice husk, Data Brief, 15 (2017) 887–895.
[32] T.M. Elmorsi, Z.H. Mohamed, W. Shopak, A.M. Ismaiel, Kinetic and equilibrium isotherms studies of adsorption of Pb(II) from water onto natural adsorbent, J. Environ. Prot., 5 (2014) 1667–1681.
[33] G. Vijaya Kumar, R. Tamilarasan, M. Dharmendira Kumar, Adsorption, kinetic, equilibrium and thermodynamic studies on the removal of basic dye Rhodamine-B from aqueous solution by the use of natural adsorbent perlite, J. Mater. Environ. Sci., 3 (2012) 157–170.
[34] S.S. Sivaprakash, S.K. Krishna, Comparative characteristic study of agricultural waste activated carbon and AC/FE3O4–nanoparticles, Int. J. Chem. Tech Res., 10 (2017) 957–963.
[35] N. Hidayah Abdullah, S. Kamyar, P. Moozarm Nia, M. Etesami, E. Chan Abdullah, Electrocatalytic activity of starch/Fe3O4/zeolite bionanocomposite for oxygen reduction reaction, Arabian J. Chem., 2017 (2017) 1–10, doi: 10.1016/j.arabjc.2017.10.014.
[36] S. Zhang, X. Zhao, H. Niu, Y. Shi, Y. Cai, Superparamagnetic Fe_3O_4 nanoparticles as catalysts for the catalytic oxidation of phenolic and aniline compounds. J. Hazard. Mater., 167 (2009) 560–566.
[37] O.E. Gutierrez-Muniz, G. Rosales, E. Ordonez Regil, Synthesis, characterization and adsorptive properties of carbon with iron nanoparticles and iron carbide for the removal of As from water, J. Environ. Manage., 114 (2013) 1–7.
[38] H.Y. Zhu, Y.Q. Fu, R. Jiang, J.H. Jiang, L. Xiao, G.M. Zeng, S.L. Zhao, Y. Wang, Adsorption removal of congo red onto magnetic cellulose/Fe_3O_4/activated carbon composite: equilibrium, kinetic and thermodynamic studies, J. Chem. Eng., 173 (2011) 494–502.
[39] S. Jorfi, S. Pourfadakari, N. Jaafarzadeh, R. Darvishi Cheshmeh Soltani, H. Akbari, Adsorption of Cr(VI) by natural clinoptilolite zeolite from aqueous solutions: isotherms and kinetics, J. Chem. Technol., 19 (2017) 106–114.
[40] M. Bhaumik, A. Maity, V.V. Srinivasu, M.S. Onyango, Enhanced removal of Cr(VI) from aqueous solution using polypyrrole/Fe_3O_4 magnetic nanocomposite, J. Hazard. Mater., 190 (2011) 381–390.
[41] X. Zhou, L.V. Bihong, Z. Zhou, W. Li, G. Jing, Evaluation of highly active nanoscale zero-valent iron coupled with ultrasound for chromium(VI) removal, J. Chem. Eng., 281 (2015) 155–163.
[42] Y.H. Liou, Sh. Lien Lo, W.H. Kuan, Ch.J. Lin, Effect of precursor concentration on the characteristics of nanoscale zerovalent iron and its reactivity of nitrate, Water Res., 40 (2006) 2485–2492.
[43] A. Morad, P. Najafi Moghadam, R. Hasanzadehb, M. Sillanpa, Chelating magnetic nanocomposite for the rapid removal of Pb(II) ions from aqueous solutions: characterization, kinetic, isotherm and thermodynamic studies, RSC Adv., 7 (2017) 433–448.
[44] S. Sepehri, M. Hei, Nitrate removal from aqueous solution using natural zeolite-supported zero-valent iron nanoparticles, Soil Water Res., 9 (2014) 224–232.
[45] M. Kashefi Asl, A.H. Hasani, E. Naserkhaki, Evaluation of nitrate removal from water using activated carbon and clinoptilolite by adsorption method, Biosci. Biotechnol. Res. Asia, 13 (2015).
[46] M. Arbabi, S. Hemati, Z. Shamsizadeh, A. Arbabi, Nitrate removal from aqueous solution by almond shells activated with magnetic nanoparticles, Desal. Wat. Treat., 80 (2017) 344–351.
[47] A. Mikhak, A. Sohrabi, M.Z. Kassaee, M. Feizian, M. Najafi Disfani, Removal of nitrate and phosphate from water by clinoptilolite-supported iron hydroxide nanoparticle, Arab. J. Sci. Eng., 42 (2017) 2433–2439.
[48] Ö. Nese, K.T. Ennil, A kinetic study of nitrite adsorption onto sepiolite and powdered activated carbon, Desalination, 223 (2008) 174–179.
[49] S.S. Tahir, N. Rauf, Thermodynamic studies of Ni(II) adsorption onto bentonite from aqueous solution, J. Chem. Thermodyn., 35 (2003) 2003–2009.
[50] A.F. Freitas, M.F. Mendes, G.L.V. Coelho, Thermodynamic study of fatty acids adsorption on different adsorbents, J. Chem. Thermodyn., 39 (2007) 1027–1037.
[51] M. Kara, H. Yuzer, E. Sabah, M.S. Celik, Adsorption of cobalt from aqueous solutions onto sepiolite. Water Res., 37 (2003) 224–232.